Lattice QCD study of three quark potential

H. Matsufuru, Y. Nemoto[a], H. Suganuma[b], T.T. Takahashi
Research Center for Nuclear Physics, Osaka University,
Mihogaoka 10-1, Ibaraki 567-0047, Japan
E-mail: matufuru@rcnp.osaka-u.ac.jp

T. Umeda
Department of Physics, Faculty of Science, Hiroshima University,
1-3-1 Kagamiyama, Higashihiroshima, 739-8526, Japan

We study the static three quark potential using lattice QCD simulation. At zero temperature, three quark potential is extracted from the baryonic Wilson loop making use of the smearing technique which enhances the ground state contribution. The potential is fitted to the phenomenological form, the sum of the Coulomb term, linearly rising term and the constant. We compare two types of the linear term, "Y" and "Δ" type, and find that the string tension almost coincide with $\sigma_{Q\bar{Q}}$ in the former case. We also investigate the three quark potential at finite temperature using the Polyakov loop correlation. In the deconfining phase, the screened potential is observed similarly to the case of $Q\bar{Q}$ system.

1 Introduction

In this paper, we present our recent result of lattice QCD calculation of the static three quark potential [1]. The static quark potential plays an important role in the phenomenological studies of hadron properties in the quark model approaches. It has been one of most vital subjects of the lattice QCD simulation to determine the potential between the static quark and antiquark [2,3]. On the other hand, the status of the static three quark potential is much less settled, in spite of its importance in the baryon spectroscopy [4,5].

It has been widely used the static Q-$\bar{Q}$ potential expressed as the sum of the short range Coulomb term and long range confining linear term. On the other hand, in the case of the three quark potential, two distinct treatments of the linear term are frequently applied. In this paper they are denoted as "Δ-type" and "Y-type" forms. The former expresses the linear potential as the sum of two-body potentials, which are proportional to the distance between each pair of quarks. The latter treats the potential with the string linking three quarks at the point with which the total length of the string takes the

[a]Present address is *Yukawa Institute for Theoretical Physics, Kyoto University, Kitashirakawa, Kyoto 606-8502, Japan.*
[b]Present address is *Tokyo Institute of Technology, 2-12-1 Ohokayama, Meguro, Tokyo 152-8551, Japan.*

minimum length, L_{min}. Y-type ansatz has been used in the phenomenological studies with the string tension $\sigma_{3Q} \simeq \sigma_{Q\bar{Q}}$, and successfully describes the gross feature of the baryon spectrum [4]. Δ-type ansatz is, however, also used in some model calculations with the string tension σ_Δ effectively around half of $\sigma_{Q\bar{Q}}$. The lattice simulations have been done mainly in 1980's [6,7,8], and there is one recent preliminary work [9]. Among them, several authors interpreted their results as the support of the Δ-type picture [6,8,9]. This embarrassing situation is mainly caused by the insufficient extraction of the ground state contribution from the baryonic Wilson loop. In nineties, calculation of Q-$\bar{Q}$ potential became much reliable by making use of the smearing technique which enhances the ground state contribution to the Wilson loop [10]. This procedure is directly applicable to the three quark system and is expected to enable the reliable extraction of the ground state contribution.

Our first goal of this work is an extraction of reliable static three quark potential using the smearing technique. With the lattice result, we discuss preferable description of the potential. These subjects are described in the next section.

Another important subject on the three quark potential is the thermal effect on it in the finite temperature QCD. Again the lattice computation is much retarded compared with the Q-$\bar{Q}$ potential. We present our preliminary result at $T > 0$ in Section 3.

2 Zero temperature result

The three quark potential is extracted from the baryonic Wilson loop,

$$W_{3Q}(\vec{r}_1, \vec{r}_2, \vec{r}_3, T) \equiv \frac{1}{3!}\epsilon_{abc}\epsilon_{a'b'c'} U_1^{aa'} U_2^{bb'} U_3^{cc'}, \tag{1}$$

$$U_k \equiv P \exp\{ig \int_{\Gamma_k} dx_\mu A_\mu(x)\}, \tag{2}$$

where P denotes the path-ordered product along the path Γ_k (k =1, 2, 3) as shown in Figure 1. The position of the contraction of three lines U_k can be chosen arbitrarily, and the result should not depend on this point. We choose the contracting point as the spatial origin, and locate three static quarks on each three spatial axis. The same constellation is averaged making use of the translational invariance.

The potential is extracted in the region where the ground state dominates in the baryonic Wilson loop,

$$\langle W_{3Q} \rangle = C_0 \exp\left[-V_{3Q}(\vec{r}_1, \vec{r}_2, \vec{r}_3)\, T\right] \qquad (T \to \infty). \tag{3}$$

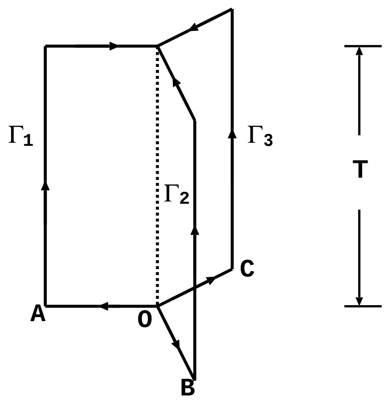

Figure 1: Baryonic Wilson loop.

At large T, however, the statistical fluctuation grows and makes reliable extraction of the potential difficult. We apply the smearing technique which enhance the ground state contribution to the Wilson loop so that the potential can be obtained at small temporal separation. The standard smearing of the Wilson loop is performed by the iterative replacement of the spatial link-variable $U_i(x)$ $(i = 1, 2, 3)$ by the obscured link-variable $\bar{U}_i(x) \in \mathrm{SU}(3)_c$[10,11] which maximizes

$$\mathrm{Re}\ \mathrm{tr}\left\{\bar{U}_i^\dagger(x)\left[\alpha U_i(x) + \sum_{j\neq i}\ \{ U_j(x)U_i(x+\hat{j})U_j^\dagger(x+\hat{i}) \right.\right. \\ \left.\left. + U_j^\dagger(x-\hat{j})U_i(x-\hat{j})U_j(x+\hat{i}-\hat{j})\}\right]\right\} \qquad (4)$$

with the smearing parameter α. The n-th smeared link-variables $U_\mu^{(n)}(x)$ $(n = 1, 2, .., N_{\mathrm{smear}})$ are iteratively defined starting from $U_\mu^{(0)}(x) \equiv U_\mu(x)$ as

$$U_i^{(n)}(s) \equiv \bar{U}_i^{(n-1)}(s) \quad (i = 1, 2, 3), \qquad U_4^{(n)}(s) \equiv U_4(s). \qquad (5)$$

The numerical simulation is done on the lattice of size $12^3 \times 24$, with the standard Wilson gauge action at $\beta = 5.7$ in the quenched approximation. We use 210 configurations generated by the pseudo-heat-bath algorithm, separated by 500 sweeps, after 5000 thermalization sweeps. The lattice spacing is determined as $a \simeq 0.19$ fm by setting the string tension of Q-$\bar{Q}$ potential to be $\sigma = 0.89$ GeV/fm. The smearing parameters are chosen as $\alpha = 2.3$, and $N_{smear} = 20$ and 12 for the Wilson loop and the baryonic Wilson loop respectively. The potentials are extracted from the (baryonic) Wilson loop by the single exponential fit in appropriate fit regions. To select the optimized smearing number and the fit ranges, we observe the ground state overlap and the "effective mass". The ground state overlap is defined as

$$C_0 \equiv \langle W_{3\mathrm{Q}}(T)\rangle^{T+1} / \langle W_{3\mathrm{Q}}(T+1)\rangle^{T}, \tag{6}$$

and estimates the overlap of the 3Q-state operator with the ground state, as discussed in the Q-$\bar{Q}$ system[11]. If the 3Q state at $t=0$ and T perfectly overlaps with the ground state, $\langle W_{3\mathrm{Q}}(T)\rangle = e^{-V_{3\mathrm{Q}}T}$ and then C_0=1 hold. (Note that $W_{3\mathrm{Q}}(T)$ in Eq.(1) is normalized as $\langle W_{3\mathrm{Q}}(T=0)\rangle = 1$.) We find C_0 is larger than 0.8 in all measured $3Q$ constellations. The "effective mass",

$$V_{\mathrm{eff}}(T) \equiv -\ln\left(\frac{\langle W_{3Q}(T)\rangle}{\langle W_{3Q}(T+1)\rangle}\right), \tag{7}$$

takes a constant value if the ground state dominates in the W_{3Q}. V_{3Q} is extracted by the single exponential fit in the fit region where the $V_{\mathrm{eff}}(T)$ exhibits a plateau.

Let us start with the Q-$\bar{Q}$ potential. Figure 2 shows the Q-$\bar{Q}$ potential obtained on our configurations. It is widely accepted that the lattice result of the static Q-$\bar{Q}$ potential is well described by the form

$$V(r) = C - \frac{A}{r} + \sigma r. \tag{8}$$

In Table 1, we list the results of the fit in three kinds of fit ranges: on-axis fit, fits with off-axis data in the whole r region and at $r \geq 2$. Since our lattice spacing is rather coarse, the fit with the off-axis data may suffer from the rotational symmetry breaking effect. This effect would be severe at short distance, where the lattice cutoff effect is large although the statistical fluctuation is small. In this sense, the fit with the on-axis data is preferable to determine the parameters. For the three quark potential, however, we inevitably treat the off-axis constellations, and then it would be meaningful to examine the typical size the rotational symmetry breaking effect in the Q-$\bar{Q}$ system. For this purpose, we carry out the fit including the off-axis data with two fit ranges. The fit using all data (all r in Table 1) results in large χ^2 value, and this is mainly caused by the result at the short distance region where the statistical error is smallest and the cutoff effect is most severe. As an alternative choice of the fit range, we instead fit at $r \geq 2$, which is more appropriate to be compared with the result of the three quark potential. In this case the fit results in $\chi^2/N_{df} = 3.3$, and we regard this value as a guide of the rotational symmetry breaking effect on this lattice. In both cases, the fit result of the Coulomb coefficient much differs from the value of on-axis fit than the case of the string tension.

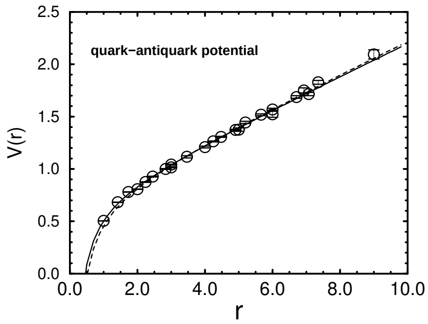

Figure 2: $Q\bar{Q}$ potential in the lattice unit. The solid and dashed lines correspond to the fit in the region of all r and $r \geq 2$ respectively.

In Figure 3, we display the lattice result of the three quark potential with two different ways corresponding to the Y- and the Δ-type ansatz respectively. The left figure is V_{3Q} vs. L_{min}, the minimum length of the flux lines linking three quarks. Three flux connecting the junction with quarks take the angles $2\pi/3$, which balances three forces with equal strength, in the case that all three angles of the "quark triangle" are less than $2\pi/3$ [4,5]. The data are fitted to the form

$$V(\vec{r}_1, \vec{r}_2, \vec{r}_3) = C_Y - A_Y \left(\frac{1}{r_{12}} + \frac{1}{r_{23}} + \frac{1}{r_{31}} \right) + \sigma_Y L_{min}. \tag{9}$$

The result is listed in Table 1. This form of the potential well describes the observed result, and the string tension is almost same as in the case of Q-$\bar{Q}$ potential. The χ^2 of the fit is in the same order as in Q-$\bar{Q}$ with fit range $r \geq 2$. Considering the rotational symmetry violation effect at this β, this seems to be a consistent result.

Alternative representation, Δ-type, is the right one in Fig. 3. The fitting function in this ansatz is

$$V(\vec{r}_1, \vec{r}_2, \vec{r}_3) = C_\Delta - A_\Delta \left(\frac{1}{r_{12}} + \frac{1}{r_{23}} + \frac{1}{r_{31}} \right) + \sigma_\Delta (r_{12} + r_{23} + r_{31}), \tag{10}$$

and the obtained parameters are also listed in Table 1. As the result of fit, we find the string tension is much smaller than the Y-type fit, although the constant and the coefficient of the Coulomb term are almost the same as the Y-type results. In the fit, σ_Δ slightly larger than the half of σ_Y. Geometrically, $2L_{min} \simeq L_\Delta = r_{12} + r_{23} + r_{31}$ roughly holds in most cases. This explains that

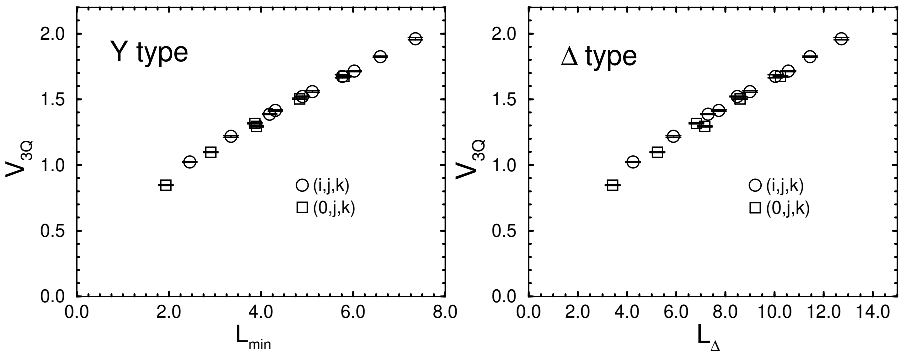

Figure 3: Three quark potential in two representations. The left figure is for the viewpoint of Y-type ansatz. L_{min} is the minimum length of the flux linking three quarks. The right figure is for the viewpoint of Δ-type ansatz with $L_\Delta = r_{12} + r_{23} + r_{31}$.

	fit range	C	A	σ	χ^2 / N_{df}
$3Q$ (Y)		0.914 (20)	0.1316(62)	0.1528(20)	$51.9/13 \sim 4.0$
$3Q$ (Δ)		0.934 (20)	0.1405(60)	0.0858(15)	$142./13 \sim 11.$
Q-$\bar{Q}$	on-axis	0.629 (16)	0.2793(12)	0.1629(47)	$1.77/3 \sim 0.59$
	all r	0.6859(71)	0.3351(55)	0.1545(20)	341./21
	$r \geq 2$	0.696 (24)	0.395 (35)	0.1561(38)	$60.0/18 \sim 3.3$

Table 1: Fit results of the Q-$\bar{Q}$ and the three quark potentials.

$\sigma_\Delta \simeq \frac{1}{2}\sigma_{Q\bar{Q}}$. On the other hand, there is another possible physical explanation for $\sigma_\Delta \simeq \frac{1}{2}\sigma_{Q\bar{Q}}$ using the $SU(3)_c$ Casimir scaling. For the Coulomb coefficient, one gluon exchange brings the color factor $1/2$ in the perturbation theory as the ratio of the $SU(3)_c$ Casimir factor. The linear term is however nonperturbative and then there is no clear explanation to keep the $SU(3)_c$ Casimir scaling beyond the perturbation. In addition, the χ^2 of the Δ-type fit is much larger than the case of the Y-type fit, where the goodness of the fit is comparable with Q-$\bar{Q}$ potential case with $r \geq 2$. Although the present simulation may suffer from rather large finite a effect, our result shows that Y-type ansatz is more preferable with the lattice data.

Our conclusion at this stage is the following. Y-type ansatz is more preferable for the lattice result although Δ-type ansatz is not completely excluded with present systematic uncertainty. Adopting Y-type picture, we have found a universal feature of the string tension as $\sigma_{3Q} \simeq \sigma_{Q\bar{Q}}$. At larger β and with improved actions, we expect the rotational symmetry gradually restored, thus observing the a dependence of χ^2 or alternative probe may give us more clear conclusion [12].

3 Finite temperature result

Now we turn on the temperature and observe how the potential changes with the thermal effect. In the last section, we found that universality of the string tension in Q-$\bar{Q}$ and $3Q$ systems almost holds with Y-type picture for the $3Q$ potential. One question is whether this relation still holds at finite temperature, especially near the critical temperature T_c. Above the T_c, the quarks and the gluons are expected to be liberated and form a plasma state, in which the potential is expected to be screened. Then one expects that the screened potential takes the Yukawa potential like as the Q-$\bar{Q}$ potential [13], and genuine three-body potential (in Y-type picture) would disappear. To observe these effects is our motivation of the finite temperature study on the static three quark potential.

On the finite temperature lattice, the static potential is extracted from the Polyakov loop correlation,

$$P_3(\vec{r}_1, \vec{r}_2, \vec{r}_3) = \langle P(\vec{r}_1) P(\vec{r}_2) P(\vec{r}_3) \rangle = c \cdot \exp(-V_{3Q}(\vec{r}_1, \vec{r}_2, \vec{r}_3) N_\tau), \tag{11}$$

where the Polyakov loop $P(\vec{x})$ is defined as $P(\vec{x}) = \mathrm{Tr} \prod_{t=0}^{N_\tau - 1} U_4(\vec{x}, t)$. The Q-$\bar{Q}$ potential is also measured in similar way.

To simulate the finite temperature system, we adopt the anisotropic lattice [14]. This has several advantages for our study. On the isotropic lattice, we need to vary β, thus the cutoff, to simulate various temperature near to T_c. The anisotropic lattice, however, enables us to work out several values of temperature without varying the lattice cutoff. On the other hand, we need the "calibration", the determination of actual anisotropy $\xi = a_\tau / a_\sigma$, which is generally deferent from the bare anisotropy γ_G in the action.

We adopt the tree level Symanzik improved action [15],

$$\begin{aligned} S_G = \quad & \beta \frac{1}{\gamma_G} \sum_{x, i<j\leq 3} \left[c_{11}(1 - P_{ij}(x)) + c_{12}(2 - R_{ij}(x) - R_{ji}(x)) \right] \\ & + \beta \gamma_G \sum_{x, i\leq 3} \left[c_{11}(1 - P_{i4}(x)) + c_{12}(2 - R_{i4}(x) - R_{4i}(x)) \right], \end{aligned} \tag{12}$$

N_t	T	#conf	fit range	C	A	σ	χ^2/N_{df}
96	$\simeq 0$	120	$r \geq 2.8$	0.1599(25)	0.0587(49)	0.01781(29)	78.1/18
28	$0.87T_c$	440	$r \geq 2$	0.2817(70)	0.119(11)	0.0089(11)	25.2/21
26	$0.93T_c$	450	$r \geq 2$	0.2934(41)	0.1253(63)	0.00638(69)	23.5/21
20	$1.22T_c$	60	-				

Table 2: Simulation parameters at finite temperature work and the result of fit of Q-$\bar{Q}$ potential to Eq. (8) below T_c. #conf denotes the number of the gauge configuration. Above T_c, the fit is carried out to the Yukawa-type form. In detail, see the text.

where $c_{11} = 5/3$ and $c_{12} = -1/12$. Plaquette $P_{\mu\nu}(x)$ and rectangular loop $R_{\mu\nu}(x)$ are defined as follows,

$$P_{\mu\nu}(x) \equiv \frac{1}{3}\mathrm{ReTr}\left[U_\mu(x)U_\nu(x+\hat{\mu})U_\mu^\dagger(x+\hat{\nu})U_\nu^\dagger(x)\right], \tag{13}$$

$$R_{\mu\nu}(x) \equiv \frac{1}{3}\mathrm{ReTr}\left[U_\mu(x)U_\mu(x+\hat{\mu})U_\nu(x+2\hat{\mu})U_\mu^\dagger(x+\hat{\nu}+\hat{\mu})U_\mu^\dagger(x+\hat{\nu})U_\nu^\dagger(x)\right].$$

The numerical calculation is done on the lattices of sizes $16^2 \times 24 \times N_t$ at $\beta = 4.56$ and $\gamma_G = 3.45$, in the quenched approximation, where N_t =96, 28, 26 and 20. They are generated with pseudo-heat-bath algorithm and separated 2000 sweeps after 20000 sweeps thermalization. The calibration is performed on the zero temperature lattice, $N_t = 96$, and results in the renormalized anisotropy $\xi = 3.95(2)$ from the Wilson loops in the spatial-spatial and temporal-spatial planes [16,17,18]. The static Q-$\bar{Q}$ potential gives the cutoffs $a_\sigma^{-1} = 1.61(1)$ GeV and $a_\tau^{-1} = 6.36(5)$ GeV. The critical temperature is estimated by the rapid change of the Polyakov loop and its susceptibility, and is found between $N_t = 24$ and 25, and slightly near to $N_t = 24$. The rough estimate of the corresponding temperatures of each N_t are summarized in Table 2 together with the number of measured gauge configurations.

Let us start with the Q-$\bar{Q}$ potential at finite temperature. The left figure of Fig 4 shows the Q-$\bar{Q}$ potential below T_c. The upper and the lower curves are at $N_t = 28$ and 26 respectively (the symbols are vertically shifted appropriately). The fit to the form (8) gives the parameters listed in Table 2 and represented as the solid line in the figure. The fit range $r \geq 2$ is selected with the same region as in the zero temperature work: we focus on the infrared feature of the potential. We note that the values in Table 2 are in the lattice unit and the cutoffs are different in spatial and the temporal directions, i.e. the potential is expressed in the unit of a_τ while the distance is in a_σ. As is seen in the Table 2, the string tension gradually decreases toward T_c [19].

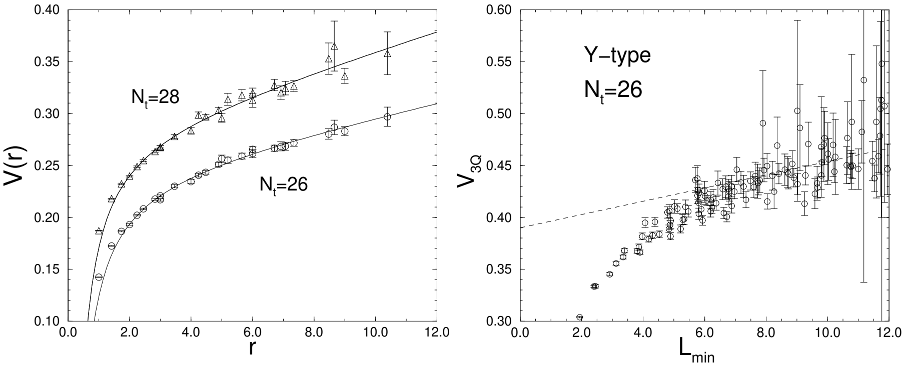

Figure 4: The left figure is Q-$\bar{Q}$ potential below T_c. The symbols are vertically shifted. The solid lines are the result of fit as listed in Table 2. The right figure is the 3Q potential at $N_t = 28$. The dashed line represents the slope of the linear term of Q-$\bar{Q}$ potential at the same N_t.

The right figure of Fig 4 shows the three quark potential at $N_t = 26$, corresponding to the confined phase near T_c, $T \simeq 0.93T_c$. The dashed line represents the linear term in Q-$\bar{Q}$ potential shifted appropriately. Although the gross feature is similar to $T = 0$ case, and the long range behavior seems consistent with the Q-$\bar{Q}$ potential, the correlator suffers from severe statistical fluctuations. Present statistics using the Polyakov loop correlator do not allow us any quantitative argument.

The potentials above T_c are displayed in Figure 5. At the long distance, The Polyakov loop correlators approach to the multiples of the expectation value of single Polyakov loop: $P_2 \to \langle P\rangle\langle P\rangle^*$ and $P_3 \to \langle P\rangle^3$. These contributions are subtracted from the potentials. The Q-$\bar{Q}$ potential above T_c is known to behave as the Yukawa-type potential [13]. In present calculation, the Debye screening mass of the Q-$\bar{Q}$ potential strongly depends on the fit range but is estimated around the $0.5 - 1$ GeV. At this N_t, we have measured the three quark potential with only equilateral constellations. In Figure 5, we compare the three quark potential divided by 3 (filled symbols) with the Q-$\bar{Q}$ potential (open symbols). We find the good agreement between the $3Q$ and the Q-$\bar{Q}$ potentials,

$$V_{3Q}(r_{12}\!=\!r_{23}\!=\!r_{31}\!=\!r) \simeq 3V_{Q\bar{Q}}(r) \qquad (T > T_c). \tag{14}$$

Above T_c, since the quarks are deconfined, there is no reason to assume that

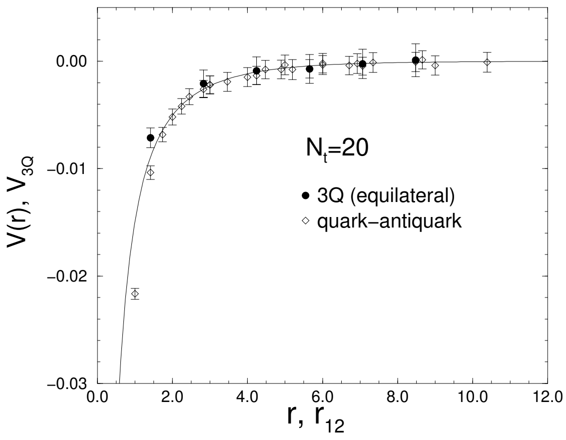

Figure 5: Q-$\bar{Q}$ (open symbols) and $3Q$ (filled) potentials at $N_t = 20$ ($T > T_c$). The $3Q$ potential is divided by 3.

the combination of quarks are in the color-singlet states. The question is whether the three quark potential can be represented as the sum of two body potential. Our present result shows that the $V_{3Q}/3$ behaves as almost same as Q-$\bar{Q}$ potential at least for the equilateral $3Q$ constellations. For more definite conclusion, we need precise results including other $3Q$ constellations and a systematic comparison between V_{3Q} and $V_{Q\bar{Q}}$ at various T.

Our finite temperature potential work has been just started and some part of the result in present report is preliminary. In particular below T_c, we need to overcome the statistics by developing the procedures. Above T_c, the signal is much more stable and quantitative understanding will be possible by systematic investigation.

Acknowledgment

The calculations have been done on NEC SX-4 at Research Center for Nuclear Physics, Osaka University and NEC HSP at INSAM (Institute for Nonlinear Science and Applied Mathematics), Hiroshima University.

References

1. T.T. Takahashi, H. Matsufuru, Y. Nemoto and H. Suganuma, Phys. Rev. Lett., in press (hep-lat/0006007).
2. G.S. Bali and K. Schilling, Phys. Rev. D 46 (1992) 2636.
3. K. Schilling, Nucl. Phys. B (Proc. Suppl.) 83-84 (2000) 140, and references therein.
4. S. Capstick and N. Isgur, Phys. Rev. D 34 (1986) 2809.
5. N. Brambilla, G.M. Prosperi and A. Vairo, Phys. Lett. B 362 (1995) 113.
6. R. Sommer and J. Wosiek, Phys. Lett. B 149 (1984) 497; Nucl. Phys. B 267 (1986) 531.
7. J. Kamesberger, G. Eder, M.E. Faber, H. Leeb and H. Markum, Proc. of "Few-Body Problems in Particle, Nuclear, Atomic and Molecular Physics"(1987) 529.
8. H.B. Thacker, E. Eichten and J.C. Sexton, Nucl. Phys. B (Proc. Suppl.) 4 (1988) 234.
9. G.S. Bali, hep-lat/0001312.
10. APE Collaboration (M.Albanese et. al.), Phys. Lett. B 192 (1987) 163.
11. G.S. Bali, C. Schlichter and K. Schilling, Phys. Rev. D 51 (1995) 5165.
12. QCD-TARO Collaboration (Ph. de Forcrand et al.), Nucl. Phys. B 577 (2000) 263.
13. M. Gao, Phys. Rev. D 41 (1990) 626.
14. F. Karsch, Nucl. Phys. B 205 (1982) 285; G. Burgers et al., Nucl. Phys. B 304 (1988) 587.
15. K. Symanzik, Nucl. Phys. B226 (1983) 187.
16. QCD TARO Collaboration (M. Fujisaki et al.), Nucl. Phys. B (Proc. Suppl.) 53 (1997) 426.
17. J. Engels, F. Karsch and T. Scheideler, Nucl. Phys. B (Proc. Suppl.) 63 A-C (1998) 427.
18. T.R. Klassen, Nucl. Phys. B 533 (1998) 557.
19. C. DeTar et al., Phys. Rev. D59 (1999) 031501.